Binary Star Measurements with the Starfire Optical Range Adaptive Optics Systems

Julian C. Christou, Jack D. Drummond, and Earl Spillar

Starfire Optical Range, U.S. Air Force Research Laboratory,
AFRL/DES, 3550 Aberdeen Ave. SE, Kirtland AFB, NM 87117-5776.
(christoj@plk.af.mil)

Abstract

Four binaries, 10 UMa, ϕ UMa, 81 Cnc, and κ UMa, were observed with adaptive optics on the 3.5m telescope at the Starfire Optical Range on March 24, 1998, in order to investigate the relative photometry produced by adaptive optics within the isoplanatic patch. Iterative Blind Deconvolution (IBD) and Parametric Blind Deconvolution (PBD) techniques were used to post-process the data, and produced consistent results for position angles, separations, and relative magnitudes. The secondary of 81 Cnc (separation = $0.12''$) appears to be 0.12 mag brighter than the primary at 0.85μ, and therefore cooler. A new orbit derived for κ UMa ($P = 35.6$ yr; $a = 0.184''$) is half the period and two thirds the size of that previously reported. Its components were separated at $0.067''$ by IBD, but not by PBD. A new orbit is also derived for ϕ UMa ($P = 79.2$ yr; $a = 0.287''$). Simulations verified the agreement produced between IBD and PBD, and overall, adaptive optics appears to be well suited for providing not only position angles and separations for close binaries, but good relative magnitudes, without quadrant ambiguity, as well.

1. Introduction

Astronomical high resolution techniques such as speckle interferometry, while providing position angle and separation information down to the telescope diffraction limit, are often incapable of providing reliable photometry, especially for close binaries or binaries with large relative magnitude differences. Adaptive optics does not always completely correct the wavefront and post-processing is often required to obtain the full information content of images, but here also the photometry may be of uncertain accuracy. In order to investigate the fidelity of photometry obtained with adaptive optics under poor and variable atmospheric conditions, high order adaptive optics (AO) images near the I band (0.85μ) of four binary stars, 10 UMa, ϕ UMa, 81 Cnc, and κ UMa, were made at the Starfire Optical Range (SOR) with the 3.5m telescope. Despite the changing point spread function (PSF) and variable loop performance, which yielded Strehl ratios on the order of 10%, relative magnitudes could be determined to ≤ 0.05 magnitudes for the first three stars, and to < 0.6 magnitudes for the extremely close pair ($0.067''$) comprising κ UMa. Position angles and separations were also obtained, and have allowed us to confirm the orbits of two of the binaries and to offer improvements for the other two.

Both Parametric Blind Deconvolution (PBD) and Iterative Blind Deconvolution (IBD) were used in post processing the data, and were mutually consistent except for κ UMa, where only IBD was able to split the pair and provide position angles, separations, and relative magnitudes. PBD and IBD analysis of computer simulations of artificial stars convolved with the observed point spread function also showed consistent results, supporting the findings obtained for the four binaries.

2. Observations

Some dozen to two dozen short exposure ($0.1-.2$sec) measurements of four binaries were made over several hours at the SOR on March 24, 1998 (adopted mean time of B1998.226), just south of Albuquerque, NM, on a less than average night, when r_0 was found to be 6.3 ± 1.7cm. Several single stars were also measured frequently and it was obvious that the seeing was highly variable due to high winds and the dome walls being up. The diffraction limit of the 3.5m telescope at 0.85μ is $0.05''$, while the expected separations ranged from 0.1-.5$''$. The V magnitudes of the four binaries ranged from 3.6 to 5.4. The 241 actuator adaptive optics system at SOR's 1.5m telescope is detailed in Drummond et al. (1998), and Lee et al (1998) and Spinhirne et al (1998) describe the 941 actuator system at the 3.5m telescope used for the observations reported here.

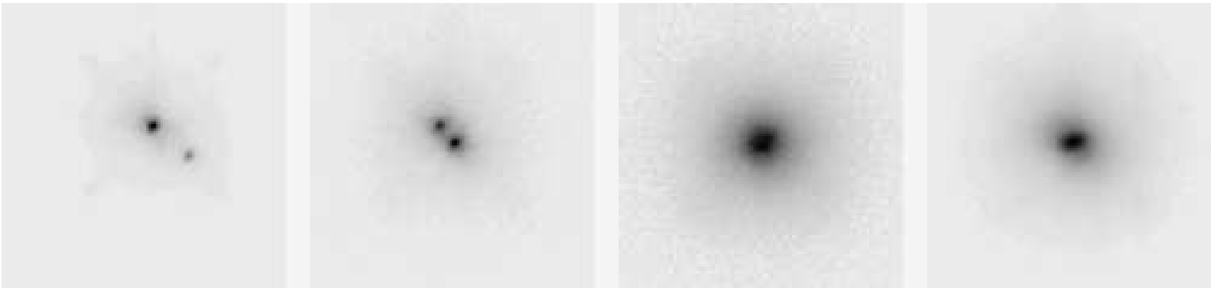

Figure 1: Four binaries observed with AO at the 3.5m telescope at the SOR. From left to right they are 10 UMa, ϕ UMa, 81 Cnc, and κ UMa. The images are displayed on a logarithmic scale, with the field being $3.3''$ wide.

Representative frames of the four binaries are shown in Fig 1. The plate scale of $0.0257''$ allowed Nyquist sampling, two pixels per resolution element.

3. Analysis

3.1 Parametric Blind Deconvolution (PBD)

All four binaries were analysed extensively with PBD. Each frame was fit for two stars modelled as two dimensional Lorentzian profiles (Drummond et al 1998; Drummond 1998). For the measured data $g(\vec{r})$ the convolution equation is

$$g(\vec{r}) = f(\vec{r}) * h(\vec{r}) \tag{1}$$

where $f(\vec{r})$ is the object distribution, $h(\vec{r})$ is the PSF or blur on the object produced by the AO system on a particular telescope, $\vec{r}$ is the spatial domain index, and $*$ denotes convolution. This is also the isoplanatic imaging equation.

For a collection of point sources, i.e. a binary or multiple star, the object can be written as

$$f(\vec{r}) = \sum_{i=1}^{N} A_i \delta(\vec{r} - \vec{r}_i) \tag{2}$$

where A_i is the amplitude of the i^{th} source at the location $\vec{r}_i = (x_i, y_i)$. At three parameters per star (A, x, and y), a binary has 6 parameters to solve for.

A PSF that can be modelled as an elliptical Lorentzian, i.e.

$$L(\vec{r}) = \frac{1}{1 + r'(\vec{r})^2} \tag{3}$$

is parameterized by three quantities, the semi-major and semi-minor axes of the ellipse and the orientation angle of the ellipse. But within the isoplanatic patch these three are the same for all stars. Thus the convolution expression (equation 1) can now be written as

$$g(\vec{r}) = f(\vec{r}) * h(\vec{r}) = \sum_{i=1}^{N} A_i \delta(\vec{r} - \vec{r}_i) * h(\vec{r}) = \sum_{i=1}^{N} A_i \delta(\vec{r} - \vec{r}_i) * L(\vec{r}) = \sum_{i=1}^{N} A_i L(\vec{r} - \vec{r}_i) \tag{4}$$

This is full Parametric Blind Deconvolution in that both object and PSF are parameterized. There are 9 parameters to be solved for in a binary star, the A, x, and y of each, and within the isoplanatic patch, the common semi-major axis, semi-minor axis, and position angle of the ellipse.

One of the advantages of parameterizing the binaries this way is that non-linear least squares can be performed, which yields for PBD not only the parameters but the errors on the parameters.

3.2 Iterative Blind Deconvolution (IBD)

If the PSF is obtained from a nearby star or from wavefront estimates, it is not necessarilly the "true" PSF for the observations. In order to minimize errors due to deconvolving by in incorrect (at some degree) PSF, "blind" deconvolution techniques can be used. Basically in "Blind" deconvolution, not only is the object unknown, but so is the PSF. By itself this represents an ill-posed problem in that there are two unknowns for one measurement. Such problems can be solved by iterative schemes when prior information concerning both object and PSF are used. This prior information is primarily that both $f(\vec{r})$ and $h(\vec{r})$ are non-negative and to a lesser extent have finite support. Another very important constraint which can be used is that of multiple observations of the same sources. This helps to break the symmetry of the problem in that for the data set, the object is common and the PSF is allowed to vary from frame-to-frame.

Iterative schemes can be applied to the solution of these unknowns. An example is that of Conjugate Gradient minimization of an error metric. The approach utilized here is that of Jefferies and Christou (1993). The error metric may be broken down into different terms. The first of these is the fidelity term which measures the "goodness of fit" between the estimates and the measure data. This can be written as

$$E_{\mathrm{F}} = \sum_{i \in R} \sum_{k} \left[g_{ik} - \left(\hat{f}_i * \hat{h}_{ik} \right) \right]^2 \cdot s_{ik} \tag{5}$$

where s_{ik} is a "bad" pixel map permitting the comparison to be made at pixels which are free from cosmic rays for example. R represents the region of support in the measurement over which the comparison is made, i represents the pixel index and k the frame index of a multiple frame data set. As can be seen from equation 1, g_{ik} is contaminated by noise so that in the limit when the estimate $\hat{g}_{ik} = \hat{f}_i * \hat{h}_{ik}$ matches the truth perfectly, then

$$E_{\mathrm{F}} = \sum_{k} \sum_{i \in R} |g_{ik} - \hat{f}_i * \hat{h}_{ik} + n_i|^2 = \sum_{k} \sum_{i \in R} |n_i|^2 = KN\sigma_n^2 \tag{6}$$

where Gaussian additive read noise with a root mean square of σ_n is assumed, N is the total number of pixels per frame and K is the total number of frames in the data set. This shows that the fidelity term has a bias associated with it due to the noise.

Non-negativity is enforced by reparameterizing both the object and PSF as their squares. The Conjugate Gradient technique minimizes the combined error metric which is written as

$$E = E_{\mathrm{F}} + \alpha_i \sum_{i} E_i \tag{7}$$

where E_i are additional possible metrics and α_i are weights for the contribution of these terms. It is noted that the choice of these weights can sometimes be arbitrary and that experience with the algorithm leads to the selection of these values.

This IBD technique is applied to sets of observations of the four binaries observed here, using a single star observation for the initial guess of the PSF. At an intermediate point the iteration is stopped, the stars are fit as Gaussians, and the iteration is continued with the initial PSF and with the newest guess for the object being the Gaussian fit. Before the iteration converges to two delta functions, the iteration is stopped and again fit for two Gaussians to provide sub-pixel locations and amplitudes which go into a binary position angle, separation and relative magnitude. The results are reported and compared to PBD below.

4. Simulations

In order to further test the consistency between IBD and PBD, two sets of binaries, wide and close, were generated as delta functions in a 512x512 array. Several sets were then convolved with observations of different single stars that were debiased of noise in the Fourier plane, and then upsampled to 512x512. The convolutions were then down-sampled to 128x128, which produced multiple frames of binary images with centers at sub-pixel locations. These sets of images were then contaminated by additive zero-mean Gaussian noise, and fit as Lorentzians (PBD), and with IBD.

Figure 2 shows the initial, intermediate, and final stages of IBD on the close pair and Fig 3 shows the IBD stages for the wide pair. Figure 4 compares the results from IBD and PBD for the close pair, and Fig 5 for the wide binary simulation. Except for perhaps a tendency for IBD to overestimate relative magnitude differences when the difference is great, IBD and PBD give consistent results for the simulations.

5. Results

Figure 6 shows the initial, intermediate, and final phases of IBD for the four binaries. Figs 7-9 show the results of each of the fits for each frame for 10 UMa, ϕ UMa, and 81 Cnc, where the IBD results are shown as open circles. Figure 10 shows the results from two IBD determinations for κ UMa, since PBD was unable to resolve the pair. Table 1 lists the results from the weighted fits from PBD for 10 UMa, ϕ UMa, 81 Cnc, and from IBD for κ UMa. Also listed are new orbital elements found by combining our measurements with those from the *'Third Catalogue of Interferometric Measurements of Binary Stars'* (McAlister et al. 1998).

Figure 11 shows the new orbits based on our observations (open circles) together with speckle interferometry data as listed by McAlister et al. 1998. The new orbits are little changed from published orbits for 10 UMa and 81 Cnc. For the latter, however, we find that the secondary is brighter than the primary at the wavelength of our observations, 0.85μ, by 0.12 magnitudes. Assuming that the primary is a G7 or G8, and adopting the photometry reported by Mason et al, then the secondary is a K1.

The last published orbit for ϕ UMa (Heintz 1971) did not include speckle data. By using only speckle and our one point, we are able to offer a new orbit derived from about half an orbit. Similarly, the last orbit for κ UMa (Morel 1970) preceded speckle, but by using speckle and our one point we find a new orbit of half the previous period. Our point is crucial because it is the first to occur after peri-apses, and helps to pin down the shorter period and smaller orbit.

Table 1: Binary Parameters (B1998.226) and New Orbits

	HR3579[a] = 10 UMa	**HR 3894**[b] = ϕ UMa	**HR 3650**[c] = 81 Cnc	**HR3594**[d] = κ UMa
PA	69.0$\pm$ 0.3	250.7 $\pm$ 0.3	121.0 $\pm$ 1.7	85.2 $\pm$ 0.3
Sep.	0.4963 $\pm$ 0.0011	0.2438 $\pm$ 0.0014	0.1224 $\pm$ 0.0010	0.0666 $\pm$ 0.0006
Δm (0.85μm)	1.68 $\pm$ 0.05	0.28 $\pm$ 0.03	-0.12 $\pm$ 0.04	0.58 $\pm$ 0.13
Element				
a	.6507 $\pm$.0018	0.287 $\pm$ .023	.1157 $\pm$ .0014	0.184 $\pm$ .002
N	204.96 $\pm$ .31	110.8 $\pm$ 19.0	318.9 $\pm$ 1.4	104.8 $\pm$ 0.6
i	130.62 $\pm$ .24	21.0 $\pm$ 3.6	124.17 $\pm$ 1.32	108.5 $\pm$ 0.8
P	21.759$\pm$ .037	79.2 $\pm$ 10.1	2.7063 $\pm$ .0027	35.612 $\pm$ .055
T_0	1993.801 $\pm$ .045	1987.2 $\pm$ .5	1979.978 $\pm$ .015	1961.15 $\pm$ .18
e	.1532 $\pm$ .0016	.324 $\pm$ .062	.431 $\pm$ .009	.551 $\pm$ .011
ω	33.67 $\pm$ .90	52.7 $\pm$ 21.4	351.2 $\pm$ 2.8	353.2 $\pm$ 2.2
Reference Orbit[e]	Harkopf *et al.* 1996	[f]	Mason *et al.* 1996	[f]

[a] Our one new point (and a different equal weighting) produces only small modification to reference orbit.
[b] The best previous orbit is from Heintz(1971), which did not include speckle data, and hence is now superseded by our new orbit with our point.
[c] Our one new point (and a different equal weighting) produces only small modification to the reference orbit, but our Δm indicates that the secondary is brighter than the primary.
[d] Best previous orbit is from Morel (1970), which did not include speckle data, and hence is now superseded by our new orbit, with our point, at half of Morel's period. IBD point indicates short period orbit, with both it and CHARA's latest point now in excellent agreement.
[e] The reference orbit is the orbit used to determine the plate scale and orientation.
[f] Reference orbit is newly determined from speckle data without our point.

6. Conclusions and Summary

The observations and simulations reported here have shown that AO can produce excellent photometry on close binary stars. Both Iterative Blind Deconvolution, where multiple frames leads to a very good object estimate and multiple frame PSF determinations, and Parameteric Blind Deconvolution, where the PSF can be modelled as function, produce consistent results on close binaries. The reason that IBD separated κ UMa ($0.067''$) was that it used multiple frames to identify the common object while attributing differences between the frames to the variable PSFs, whereas PBD measured each frame independently, no single one of which showed the two stars. Thus all three quantities, position angles, separations, and relative magnitudes without quadrant ambiguity can routinely be gleaned from AO images.

Two of the binaries, 10 UMa and 81 Cnc, appear to be on schedule according to their latest orbits, with the secondary of 81 Cnc being brighter than the primary at 0.85μ, and therefore cooler. By including speckle interferometry with our AO data, new orbits for ϕ UMa and κ UMa have been derived, with an orbit period half of that derived previously for the latter.

References

Drummond, J.D., Fugate, R.Q., Christou, J.C., and Hege, E.K. (1998). *Icarus* **132**, p80.
Drummond, J.D. (1998). *SPIE* **3353**, p1030.
Hartkopf, W.I., Mason, B.D., and McAlister, H.A. (1996). *AJ* **111**, p370.
Heintz, W.D. (1971). *AJ* **76**, p277.
Jefferies, S.M. and Christou, J.C. (1993). *ApJ* **415**, p862.
Lee, D., Ellerbroek, B., and Christou, J.C. (1998). *SPIE* **3353**, p1080.
Mason, B.D., McAlister, H.A., and Hartkopf, W.I. (1996). *AJ* **112**, p276.
McAlister, H.A et al. (1998). http://www.chara.gsu.edu/DoubleStars/Speckle/cat3.
Morel, P.J. (1970). *A& A SS* **1**, p429.
Spinhirne, J.M. et al. (1998). *SPIE* **3353**, p22.

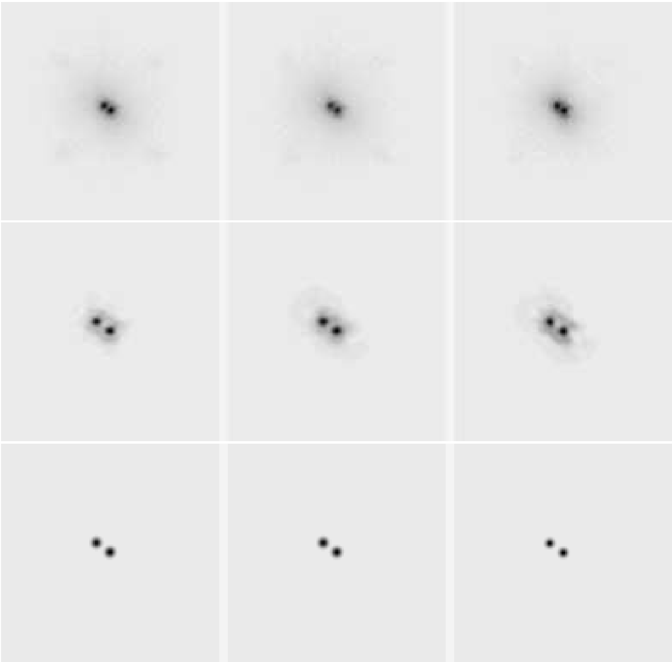

Figure 2: Close binary simulation. Top to bottom: Initial results (at original scale), intermediate Gaussian fits, final results.

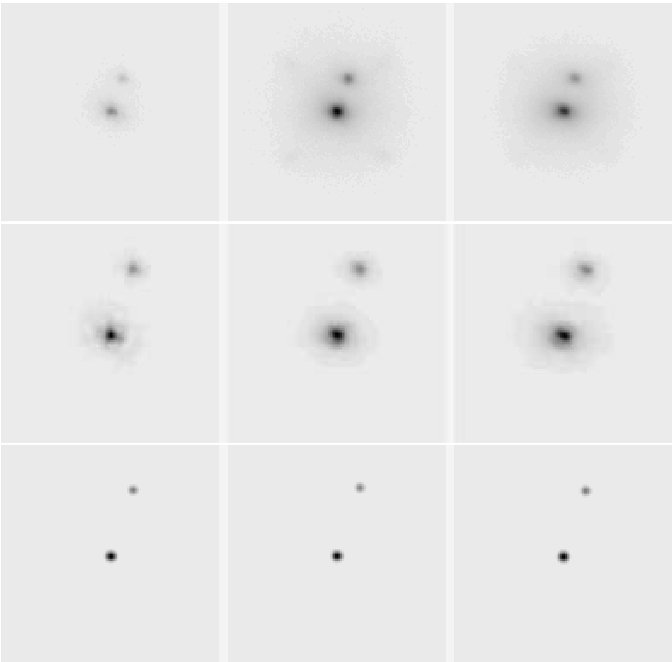

Figure 3: Wide binary simulation: Top to bottom: Initial results (at original scale), intermediate Gaussian fits, final results.

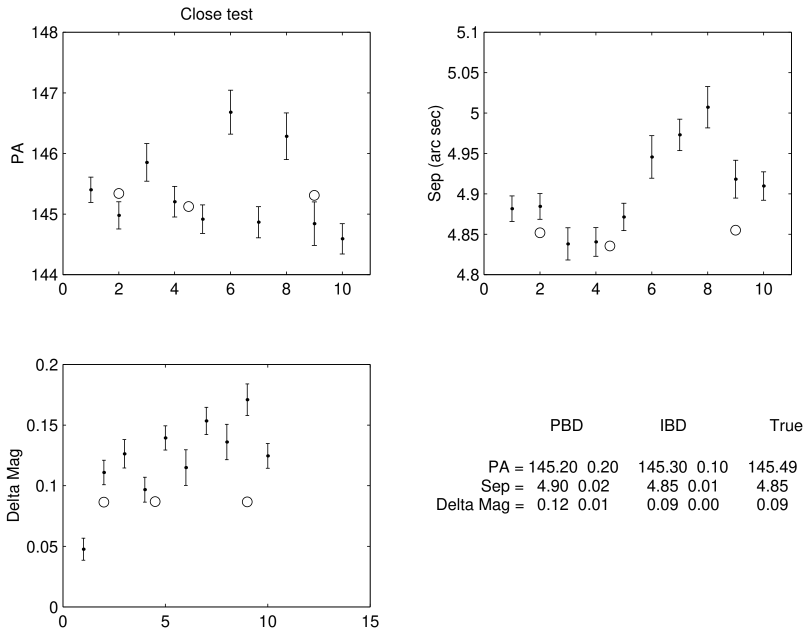

Figure 4: Close binary simulation comparison of IBD (open circles) and PBD (error bars).

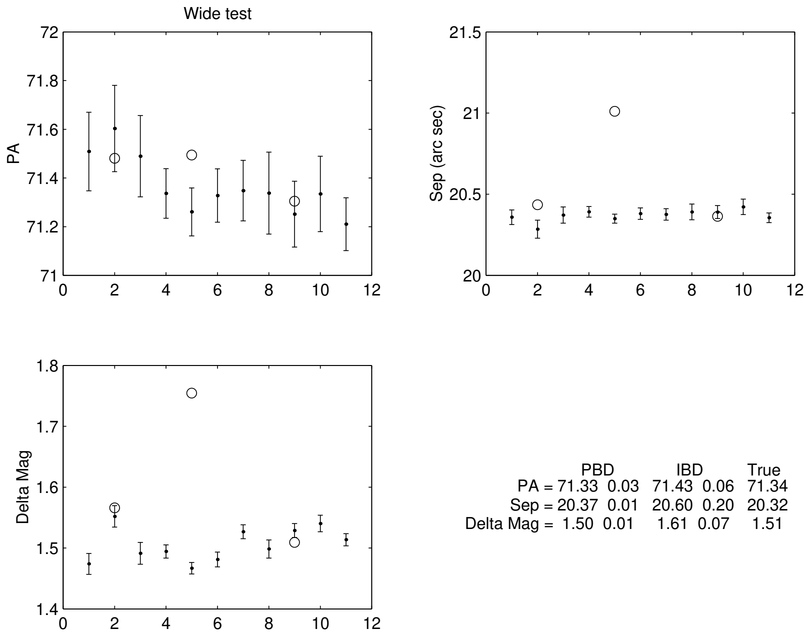

Figure 5: Wide binary simulation comparison of IBD and PBD.

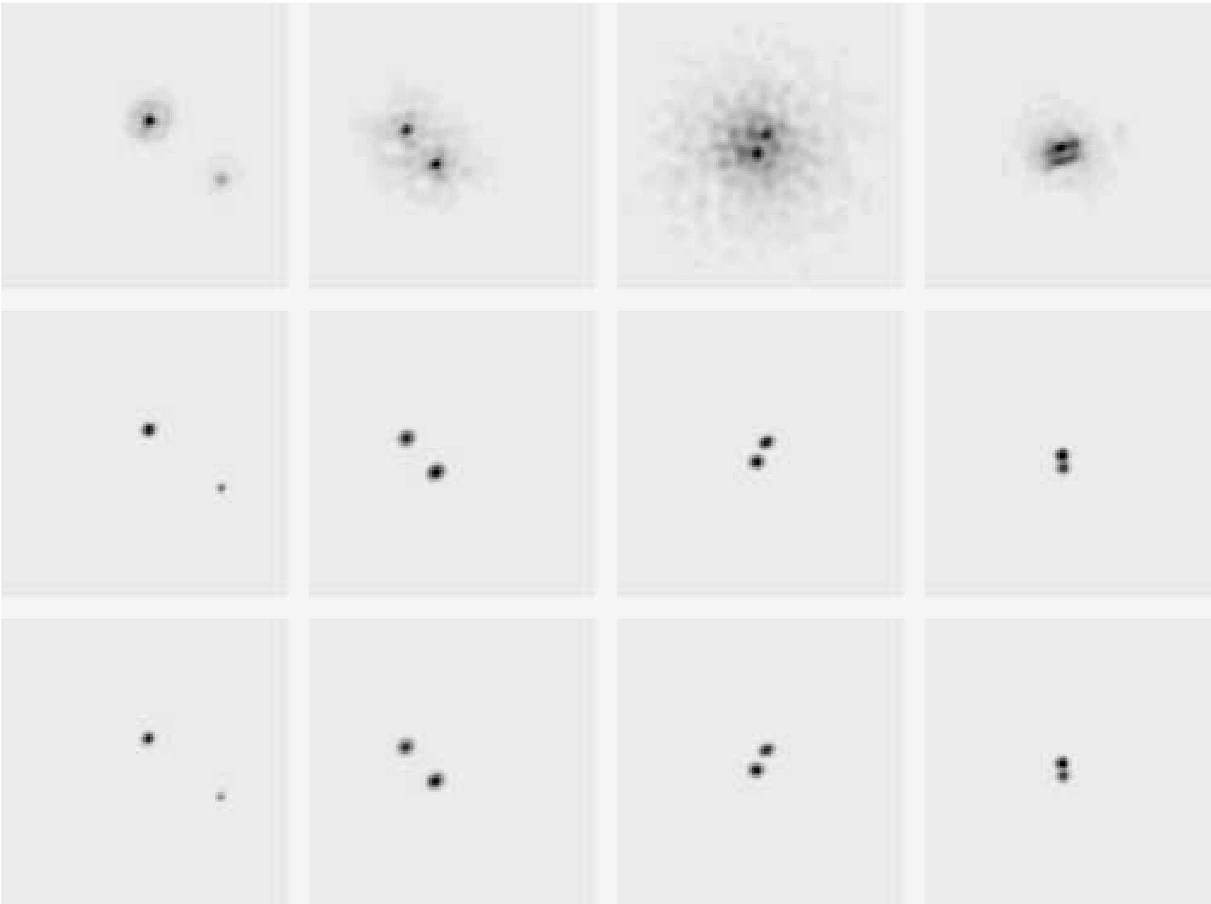

Figure 6: Initial, intermediate Gaussian, and final result of IBD of the four binaries. From left to right are 10 UMa, ϕ UMa, 81 Cnc, and κ UMa.

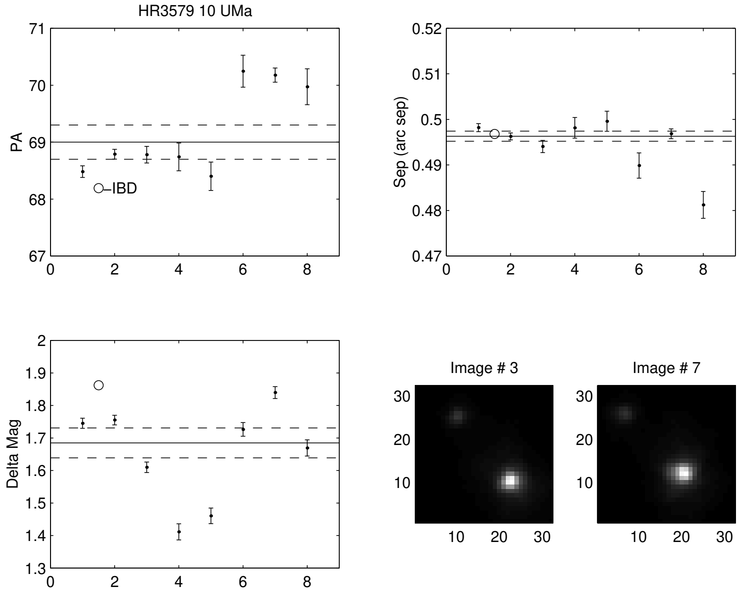

Figure 7: Relative magnitudes, position angles and separations for HR3579 (10 UMa). Errorbars on the points are from PBD analysis. The weighted mean of the measurements are shown as a solid line, and the associated error of this mean is shown as a dashed line above and below. IBD results are shown as open circles. Images are dispayed on a linear scale.

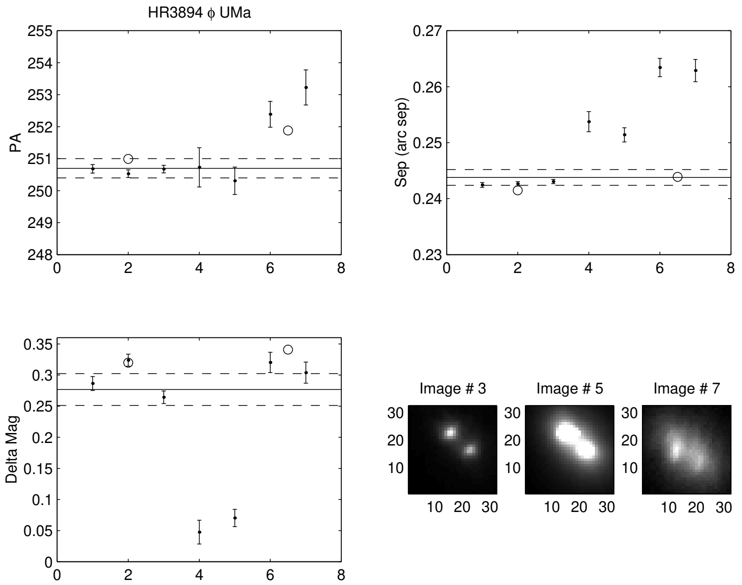

Figure 8: Same as Fig 6, but for HR3894 (ϕ UMa).

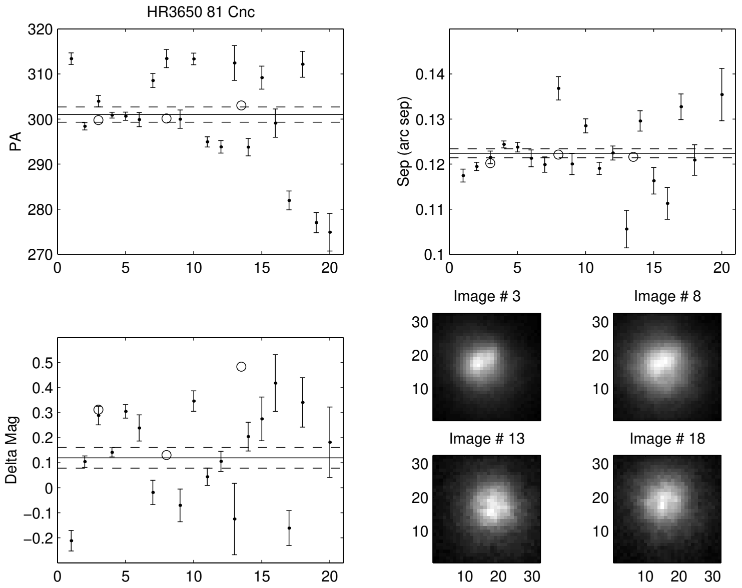

Figure 9: Same as Fig 6, but for HR3650 (81 Cnc).

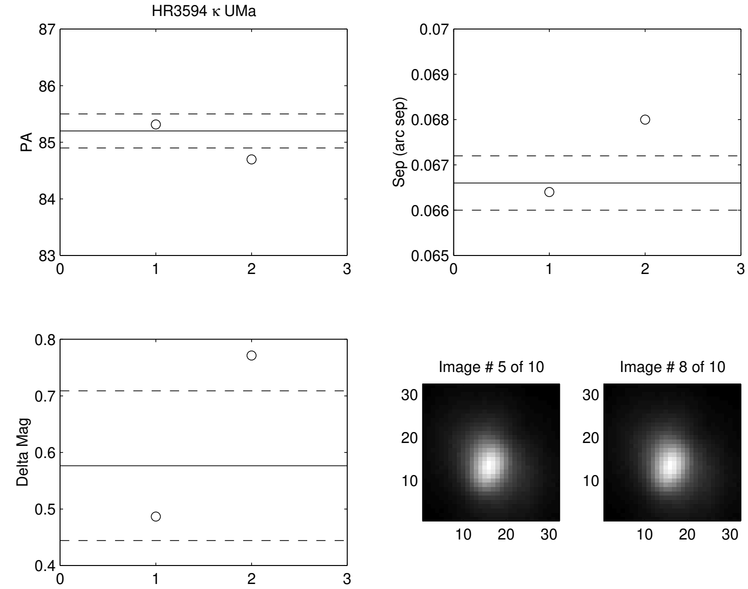

Figure 10: Relative magnitudes, position angles and separations for HR3594 (κ UMa) from IBD. PBD failed to split HR3594, so only IBD results are shown. This is the only binary for which the weighted standard deviation from IBD results is depicted.

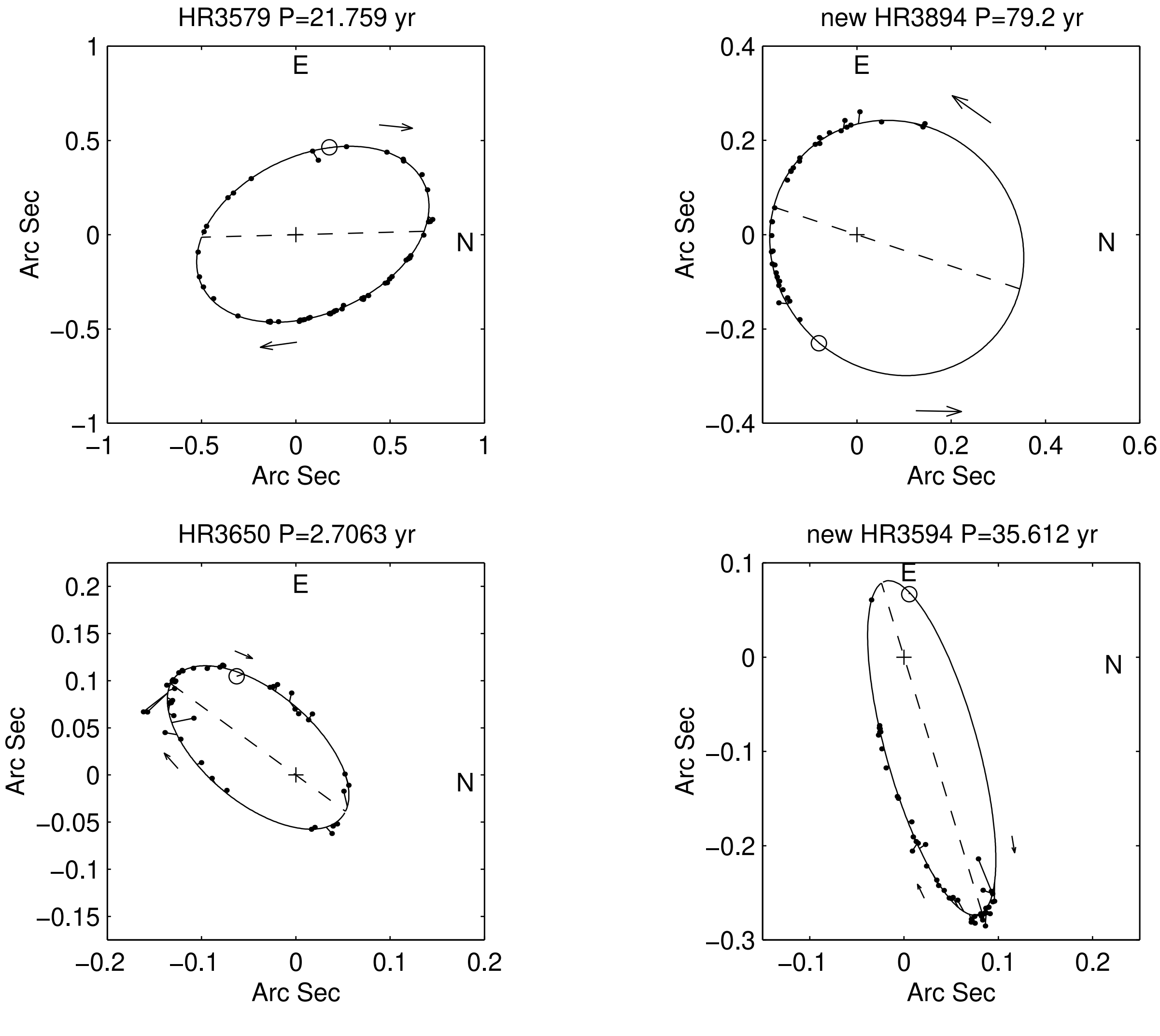

Figure 11: New binary orbits. Our observations are depicted by open circles at B1998.226. All others are speckle interferometry measurements listed by McAlister et al.